Available online at www.sciencedirect.com
ScienceDirect
C. R. Physique 10 (2009) 437–446
COMPTES RENDUS PHYSIQUE

Metamaterials / Métamatériaux

Negative bending mode curvature via Robin boundary conditions

Samuel D.M. Adams [a], Richard V. Craster [b], Sébastien Guenneau [c,*]

[a] *Department of Mathematics, Imperial College London, London SW7-2AZ, UK*
[b] *Department of Mathematical and Statistical Sciences, University of Alberta, Edmonton, Canada, T6G 2G1*
[c] *Department of Mathematical Sciences, Liverpool University, Liverpool L69-3BX, UK*

Available online 9 May 2009

Abstract

We examine the band spectrum, and associated Floquet–Bloch eigensolutions, arising in straight walled acoustic waveguides that have periodic structure along the guide. Homogeneous impedance (Robin) conditions are imposed along the guide walls and we find that in certain circumstances, negative curvature of the lowest (bending) mode can be achieved. This is unexpected, and has not been observed in a variety of physical situations examined by other authors. Further unexpected properties include the existence of the bending mode only on a subset of the Brillouin zone, as well as permitting otherwise unobtainable velocities of energy transmission. We conclude with a discussion of how such boundary conditions might be physically reproduced using effective conditions and homogenization theory, although the methodology to achieve these effective conditions is an open problem. ***To cite this article: S.D.M. Adams et al., C. R. Physique 10 (2009).***

Résumé

Conditions de Robin pour modes de flexion à dispersion négative. Nous étudions le spectre de bande associé aux modes de Floquet–Bloch dans des guides d'ondes planaires acoustiques périodiques. Nous imposons des conditions d'impédance homogènes (conditions de Robin) sur les bords du guide d'épaisseur finie, et observons dans certains cas une courbure négative de la première bande de dispersion (mode de flexion). Cette trouvaille est pour le moins inattendue, car une telle anomalie n'a pas été reportée à ce jour pour d'autres types de conditions limites dans nombre de problèmes physiques. Encore plus surprenante est l'existence de modes de flexions dans un segment de la zone de Brillouin ainsi que des vitesses de groupe extrêmes. Finalement, nous suggérons certaines pistes pour obtenir de telles conditions d'impédances, telle que la voie classique de l'homogénéisation, même si cela reste pour l'heure un problème ouvert. ***Pour citer cet article : S.D.M. Adams et al., C. R. Physique 10 (2009).***

Keywords: Robin conditions; Negative refraction; Sub-wavelength imaging

Mots-clés : Conditions de Robin ; Réfraction négative ; Imagerie haute résolution

* Corresponding author.
E-mail addresses: samuel.adams@imperial.ac.uk (S.D.M. Adams), craster@ualberta.ca (R.V. Craster), guenneau@liverpool.ac.uk (S. Guenneau).

1631-0705/$ – see front matter
doi:10.1016/j.crhy.2009.03.009

Version française abrégée

Nous considérons un guide planaire périodique dont la géométrie est décrite dans la légende de la Fig. 1. Les ondes acoustiques qui s'y propagent sont solutions de l'équation de Helmholtz (1) dans les couches homogènes $j = 1$ et 2 occupées par des matériaux élastiques isotropes de densités ρ_j kg m^{-3} où les vitesses des ondes acoustiques sont de $c_T(j)$ m s^{-1}. Les paramètres géométriques et physiques sont normalisés par rapport à l'épaisseur h du guide et ceux du matériau 1. Nous imposons des conditions d'impédance (de Robin) $\frac{\partial u}{\partial n} + \mu_{\pm} u = 0$ sur les paroies horizontales supérieure et inférieure $y = \pm 1$ du guide planaire. Par ailleurs, des conditions classiques de continuité du champ de déplacement et de la composante normale du stress sont imposées aux interfaces verticales entre les différents matériaux de la cellule élémentaire et des conditions de Floquet–Bloch sur les bords gauche et droit de celle-ci. Nous nous intéressons plus particulièrement au cas où les conditions d'impédance sont de signes opposés i.e. $\mu_+ \mu_- < 0$.

En premier lieu, nous considérons le problème homogène et obtenons la relation de dispersion (6) qui se réduit au cas Neumann [5] pour $p = 0$, car dans ce cas la seule solution non-triviale du problème est pour $\mu = 0$.

En second lieu, nous considérons le problème multi-couches et obtenons la relation de dispersion (7), (8) qui est identique au cas Dirichlet [5]. Le spectre de bande de notre guide avec conditions d'impédance contient donc en particulier celui du guide avec conditions de Dirichlet, mais il est plus riche. En effet, les courbes en pointillé sur la Fig. 4 n'existent que pour les conditions d'impédance, alors que les courbes continues existent dans les deux cas. On note par ailleurs que la première courbe de dispersion a une courbure négative et elle n'existe que pour un petit interval de la zone de Brillouin. En jouant sur la valeur de l'impédance, nous obtenons des courbes de dispersion exotiques reportées sur la Fig. 5. Pour le cas $\mu = 10$, nous observons dans la Fig. 6 que le premier mode de flexion admet une courbure négative avec une pente quasi-infinie quand $k_0 d = 2.9$. Ce type de dispersion anormale pourrait avoir des applications non seulement en réfraction négative, mais aussi dans le transport ultra-rapide de l'énergie. Nous analysons dans la Fig. 7 l'extension du support des modes de flexion en fonction de la valeur de l'impédance. Ce type de mode n'existe que sur des sous-ensembles strictement inclus dans la zone de Brillouin, contrairement aux conditions au bord classiques de type Dirichlet ou Neumann. Enfin, nous reportons dans la Fig. 8 des profils du champ de déplacement.

Nous concluons notre étude par les applications qui peuvent-être envisagées, telles que la réalisation d'endoscopes à haute résolution. Nous étayons ces perspectives par des résultats numériques illustrant le principe de tels endoscopes dans la Fig. 9, même si nous ne sommes pas en mesure de démontrer l'aspect haute-résolution.

1. Introduction

Negative refraction [1] is a rapidly growing field in photonics, which started back in 2000 with the controversial claim of Sir John Pendry that it leads to the possibility of a lens displaying sub-wavelength imaging [2] which is an electromagnetic paradigm [3]. The quest for this superlens fueled research in this area, which lies somewhere at the interface between surface science, photonics and new technologies, and a comprehensive review of its infancy can be found in [4]. We are concerned today with acoustical counterparts of perfect lenses [5], having tomographic applications in mind, but also slow wave devices in the spirit of what has been achieved in photonic crystals [6,7], but transposed to the area of acoustic delay lines [8]. Thus far, Neumann (freely vibrating) and Dirichlet (clamped) conditions (or an alternation of them) were assumed to hold on the walls of one-dimensional strips, while in the present paper we investigate the possibility of impedance (Robin) boundary conditions. Such conditions might arise in a number of physical situations, including rough or high-contrast structured interfaces [9], but importantly also electrical circuits [10]. The propagation of waves with anti-parallel group and phase velocities was discussed in the late 1940s by Brillouin [11] and Pierce [12] who utilized a series-capacitance/shunt-inductance equivalent circuit model supporting backward waves, see panel (a) of Fig. 1. However, such circuits were dominated by diffraction-scattering phenomena, as these were used in the Bragg regime, whereby the wavelength is comparable to the unit cell repeated periodically. In contrast, circuit-based electromagnetic metamaterials displaying negative refraction through effective impedance conditions operate at low frequency, in the fundamental mode of the waveguide when dissipative effects are much smaller, see [10]. In that case, diffraction-scattering phenomena can be neglected, leading to non-intuitive effective properties such as interfaces now known to support plasmon waves which are responsible for the enhancement of evanescent waves in metamaterials [13].

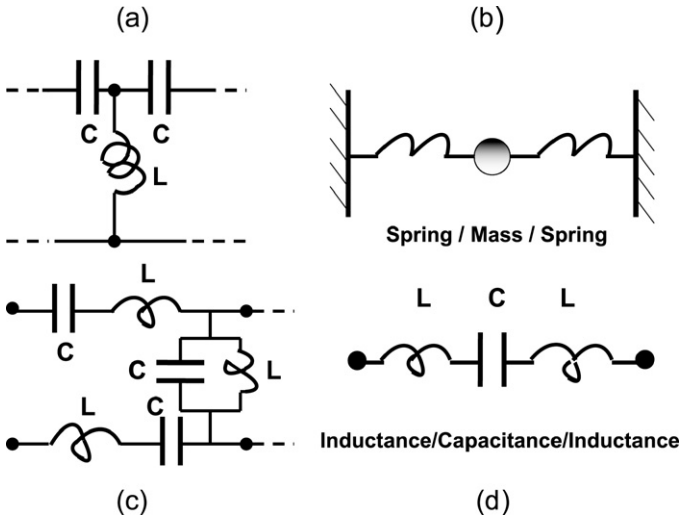

Fig. 1. Fundamentals of transmission lines and acoustic resonators. Panel (a) displays an infinite periodic circuit consisting of an alternation of capacitances on its upper wall and inductances on its vertical walls (which was shown to support backward waves in the Bragg regime by Brillouin [11]); Panel (b) shows an acoustic resonator consisting of a mass connected to two springs attached to clamped walls on either side (acoustic equivalent [18] of a split ring resonator displaying artificial magnetism in electromagnetic meta-materials [14]); Panel (c) is a unit cell of an infinite periodic circuit extending some designs of Caloz and Itoh for negatively refracting transmission lines in the homogenization regime [10] (note that effective impedance conditions on upper and lower walls should be of opposite signs from asymmetry considerations); Panel (d) draws a parallel with the acoustic resonator of panel (b).

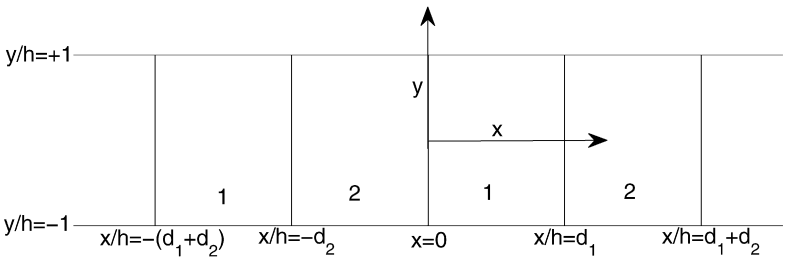

Fig. 2. The infinite periodic waveguide; materials 1 and 2 are shown. The guide occupies $-\infty < x/h < \infty$, $-1 < y/h < +1$.

Interestingly, impedance conditions of the Robin type such as those discussed in the current paper arise naturally in transmission lines consisting of asymmetric resonating electrical circuits exhibiting some negative refraction in the quasi-static regime [10]. This asymmetry allows for oppositive propagation directions for surface waves supported by upper and lower walls of the waveguide (backward and forward). This leads to a most unusual imaging system whereby the source feeds the image and vice versa, which somewhat echoes a proposal of a perfect lens by Pendry and Ramakrishna using an alternation of layers with negative refractive index (NRI) and positive refractive index *with gain* to compensate for the absorption inherent in NRI. However, the present paper focusses on the area of acoustic waveguides where the mathematical models and the underlying physics is much different. We hope that our results on negatively refracted low frequency bending modes will open new routes in delay lines and imaging devices displaying high-resolution.

Fig. 2 shows the geometry of the guide we consider. The solutions in the periodic guide are characterized by the frequency, ω, and the product of the Bloch wave number, k_0, with the periodic cell length d. The spectral problem does not permit propagating solutions for some range of frequencies and so-called stop bands, [16], occur and we investigate the appearance of these. Impedance boundary conditions are imposed on the upper and lower guide walls and we demonstrate that negative group velocity of the bending mode can occur. It can be demonstrated, [5], that such phenomena are not possible in the analogous cases of homogeneous Dirichlet or Neumann wall conditions. Further, this has not previously been observed in curved guides or guides with alternating boundary conditions. It should be

noted that the appearance of this phenomena is of considerable practical interest [6,7], in particular in its potential for opening new possibilities for sub-wavelength imaging. Further, we note some curves also have very slight curvature in the ω, k_0 plane and allow for some very slow propagation of energy, as was observed in the Dirichlet and Neumann cases [5].

We begin by formulating the problem and deriving the modal solution for the impedance system. A dispersion relation is given, but we later find that this captures only part of the solution. We offer a comparison with the analogous Dirichlet and Neumann problems, and outline why the argument which prohibits negative bending mode curvature in those cases does not apply here. Results are presented for the fundamental cases of interest, and we investigate the variation of the bending mode as boundary conditions are altered. There are physical implications of the anomalous dispersion and trapping phenomena that we discuss. We finally propose a design of an acoustic endoscope via anomalous dispersion.

2. Formulation

We consider a striped guide occupying $-1 < y/h < 1$, $-\infty < x/h < +\infty$, shown in Fig. 2. We assume material 1 occupies regions $nd < x/h < nd + d_1$, and material 2 occupies regions $nd + d_1 < x/h < (n+1)d$, for all integers n, and this enables us to solve the problem on region $0 < x/h < d$, subject to Bloch conditions. Impedance conditions on the guide walls are imposed and we permit differing impedance parameters on top and bottom. Here and henceforth a j in subscript will denote a material parameter or variable corresponding to, or only defined in, material j, for $j = 1, 2$.

We non-dimensionalize throughout using parameters of material 1; all variables and parameters decorated with tilde are non-dimensional. The following non-dimensional variables and parameters are introduced:

$$\tilde{x} = x/h, \quad \tilde{y} = y/h, \quad \tilde{t} = c_{T(1)}t/h, \quad \tilde{u}_3 = u_3/h, \quad \tilde{\tau}_{ik} = \tau_{ik}/\left(\rho_{(1)}c_{T(1)}^2\right)$$
$$\tilde{\omega} = h\omega/c_{T(1)}, \quad \tilde{\alpha}_{(j)} = c_{T(j)}/c_{T(1)}, \quad \tilde{\beta}_{(j)} = \rho_{(j)}/\rho_{(1)}$$

for $j = 1, 2$. In subsequent equations, the tilde will be omitted for convenience, and everything hereafter is non-dimensional. The Helmholtz equations are:

$$\alpha_{(j)}^2\left(\frac{\partial^2 u_3^{(j)}}{\partial x^2} + \frac{\partial^2 u_3^{(j)}}{\partial y^2}\right) + \omega^2 u_3^{(j)} = 0 \tag{1}$$

and the equations are valid within the domains occupied by materials $j = 1, 2$.

Impedance boundary conditions of the Robin type

$$\frac{\partial u}{\partial n} + \mu_{\pm} u = 0 \tag{2}$$

are applied along the guide walls $y = \pm 1$, and interface conditions ensuring the continuity of normal stress and displacement at material junctions are imposed.

The change of phase between $x = 0$ and $x = d$ is fixed using Floquet–Bloch conditions on the normal stress and displacement:

$$u_3^{(2)}(x = d^-) = u_3^{(2)}(x = 0^-)\exp(\mathrm{i}k_0 d), \qquad \tau_{13}^{(2)}(x = d^-) = \tau_{13}^{(2)}(x = 0^-)\exp(\mathrm{i}k_0 d) \tag{3}$$

and to ensure propagating solutions we impose that k_0 is real.

Fig. 3 shows the Bloch spectrum when $\mu_- = \mu_+ = 1$ for a guide made of aluminum–tin (materials 1 and 2 respectively: aluminum has $c_T = 3130$ m/s and $\rho = 2700$ kg/m^3 and tin has $c_T = 1670$ m/s and $\rho = 7300$ kg/m^3), and with $d_1 = d_2 = 3$. All subsequent computations will use the same material parameters and layer thicknesses. In this instance, the spectrum resembles that of the analogous clamped case. In particular, a stop band at zero frequency appears, and several band gaps form. Further, we note the presence of two nearly completely flat bands associated with modes trapped in the layers, at $\omega = 1.17$, $\omega = 1.39$. We do not present a full comparison between the impedance problem and clamped/free problems here, but instead proceed directly to the special case in which negative bending mode curvature can be obtained.

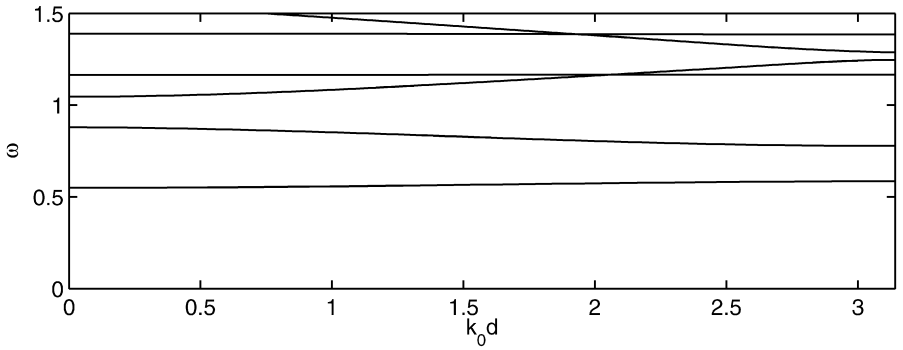

Fig. 3. The Bloch spectrum for the impedance problem in which $\mu_- = \mu_+ = 1$.

Here and henceforth we shall restrict analysis to the special case in which $\mu = +\mu_+ = -\mu_-$. We begin by examining the homogeneous problem in which one can pose a single-mode solution in each of the materials of the form:

$$u_3^{(j)}(x, y) = \left[A_j \exp(+\mathrm{i}k_{n(j)}x) + B_j \exp(-\mathrm{i}k_{n(j)}x)\right]\hat{u}_{3n}^{(j)}(y), \quad \text{for } j = 1, 2 \tag{4}$$

valid for $k_{n(j)} \neq 0$, in which A_1, A_2, B_1, B_2 are constants, and $\hat{u}_{3n}^{(j)}(y)$ is the nth modal solution:

$$\hat{u}_{3n}^{(j)}(y) = \left[\mu \sin(p_{(j)}) + p_{(j)} \cos(p_{(j)})\right]\cos(p_{(j)}y) + \left[p_{(j)} \sin(p_{(j)}) - \mu \cos(p_{(j)})\right]\sin(p_{(j)}y) \tag{5}$$

in which $p_{(j)} = (\omega^2/\alpha_{(j)}^2 - k^2)$.

Invoking a determinant condition shows that boundary conditions impose:

$$\mu p_{(j)} \sin(p_{(j)}) \cos(p_{(j)}) = 0 \tag{6}$$

thus possible solutions are at $p_{(j)} = \pi/2, \pi, 3\pi/2, \ldots$, provided $\mu \neq 0$. The case $p_{(j)} = 0$ leads to the trivial solution, unless $\mu = 0$, which corresponds to the bending mode in the stress-free case.

3. Results

We now turn our attention to the layered case, and note that as in previous acoustic problems, the modal solution does not include material parameters. This opens the possibility for single mode into single mode (monomodal) transmission between layers, in which a separable solution is applicable. In this instance one arrives at a dispersion relation without requiring the modal solution $u_j^{(n)}(y)$:

$$2r\left(\cos(k_{n(1)}b)\cos(k_{n(2)}a) - \cos(k_0 d)\right) - \left(1 + r^2\right)\sin(k_{n(1)}b)\sin(k_{n(2)}a) = 0 \tag{7}$$

$$r = \left(\alpha_{(2)}^2 \beta_{(2)}\right)/\left(\alpha_{(1)}^2 \beta_{(1)}\right)\sqrt{\frac{\alpha_{(2)}^{-2}\omega^2 - (n\pi/2)^2}{\alpha_{(1)}^{-2}\omega^2 - (n\pi/2)^2}} \tag{8}$$

valid for $n = 1, 2, \ldots$. The above dispersion relation, known as the Kronig–Penney relation in the context of electrons in solids [17], naturally appears in one dimensional photonic and phononic crystals (with layers of infinite height), see e.g. [16,19,20] and references therein. This is the same as in the clamped case, and thus the Bloch spectrum for the impedance problem must contain the spectrum for the clamped problem. It follows that the analysis of that problem concerning the existence of slow modes also holds here, [5]. The impedance-problem, however, has a wider Bloch spectrum, and this is demonstrated in Fig. 4, in which $\mu = 1$, and where solutions corresponding to both clamped and impedance problems are shown as solid lines, and solutions corresponding to the impedance case only are shown as dashed lines. Due to the inclusion of these spectra, it is clear that the impedance guide supports energy propagation at more frequencies than the analogous clamped guide. Furthermore, Fig. 4 shows that modes of the layered structure exist below the $n = 1$ cut-off frequency of both materials, at $\alpha_{(1)}\pi/2 = 1.57$, $\alpha_{(2)}\pi/2 = 0.84$. The figure shows a bending mode with negative curvature, which exists in $0 < k_0 d < 0.283$, and we draw attention to this in panel 4(b).

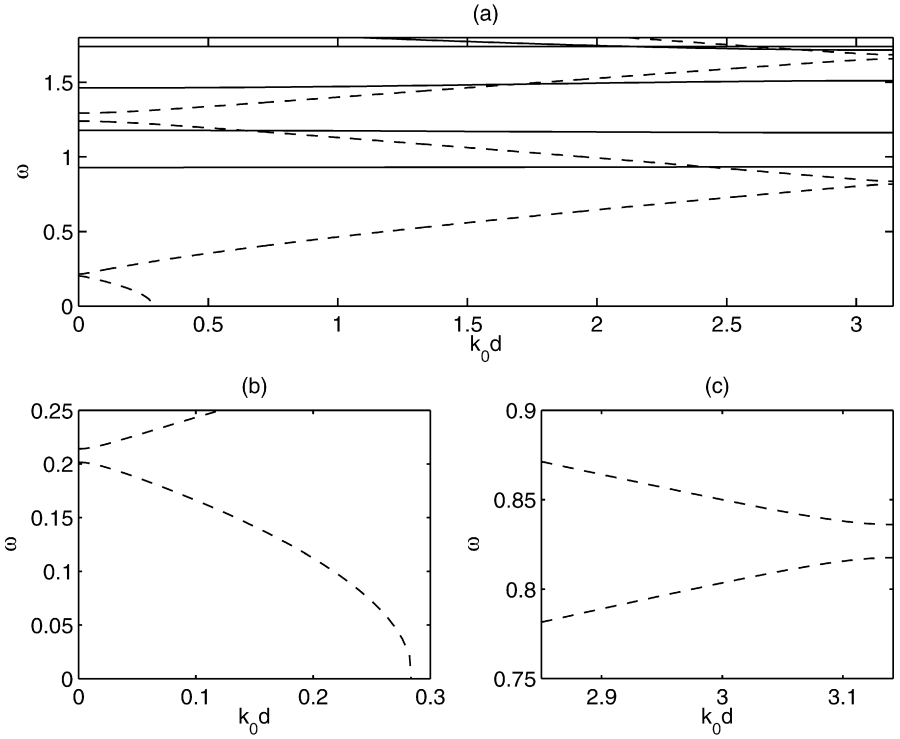

Fig. 4. The Bloch spectrum for $\mu = +\mu_+ = -\mu_- = 1$ is shown as solid curves (clamped and impedance spectra) and dashed curves (impedance only spectrum). Panel (b) highlights that the lowest mode exists only on a subset of $0 \leqslant k_0 d \leqslant \pi$, and that negative curvature is observed. Panel (c) shows that bandgaps also form in the impedance-only spectrum.

Panel 4(c) shows that stop bands form in the impedance only spectrum, preventing energy propagation at a range of frequencies. In a similar fashion to the traction-free problem, these bands generally widen as material disparity increases.

We briefly address these additional modes, and explain why they are not captured by the derived dispersion relation, (7). In deriving (7) it was assumed that a single modal expansion can be posed in each material, and continuity conditions imposed on those expansions will yield a dispersion relationship. However, it is only by virtue of a biorthogonality relationship, [15], which takes a much simpler form in acoustics, that one can be sure that mode scattering will not occur. In the problem at hand, the biorthogonality property is lost, and modes scatter, whenever the mode number n is odd in one material and even in the other. In this case, as happens with the bending mode, there is no governing dispersion relation and hence no analytical tools are available. In particular, the analysis presented in [5], which demonstrates that the clamped guide bending mode always has positive group velocity involves perturbing the derived dispersion relationship. When impedance conditions are used, however, the bending mode is not a solution of (7), and so the possibility for negative bending mode curvature remains open.

We now examine how the response of the bending mode varies as the impedance parameter, μ, is changed. It is clear that $\mu = 0$ and $\mu = \infty$ correspond to traction-free and clamped problems respectively, and in the absence of any physical mechanism to introduce a discontinuity it is natural to expect to find a smooth transition as those values are approached.

We begin by giving the Bloch spectrum of bending modes for various values of μ, shown in Fig. 5. There are three types of bending mode available, and in all cases the group velocity is either positive or negative on the entire support; a feature characteristic of straight walled acoustic guides. Modes supported on $k_0^* d < k_0 d < \pi$ appear, for which $k_0^* > 0$, and these modes have positive group velocity throughout, henceforth referred to as type I modes. Fig. 5 shows such examples of such modes at $\mu = 0.2$ and $\mu = 2.5$. We also note that $k_0^* \to 0$ as $\mu \to 0$, and the mode shown at $\mu = 0.2$ continuously deforms into the bending mode of the traction-free problem, supported on all of $0 < k_0 d < \pi$, with positive group velocity. Modes supported on $0 < k_0 d < k_0^* d$ appear, for which $k_0^* d < \pi$, and these have negative

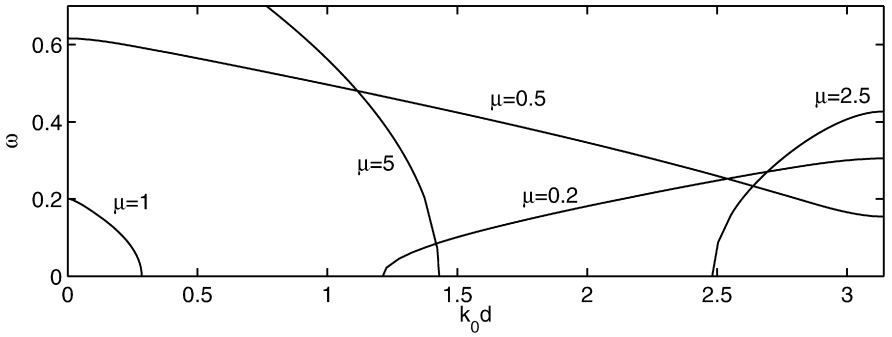

Fig. 5. The Bloch spectrum for the bending modes for a variety of values of μ.

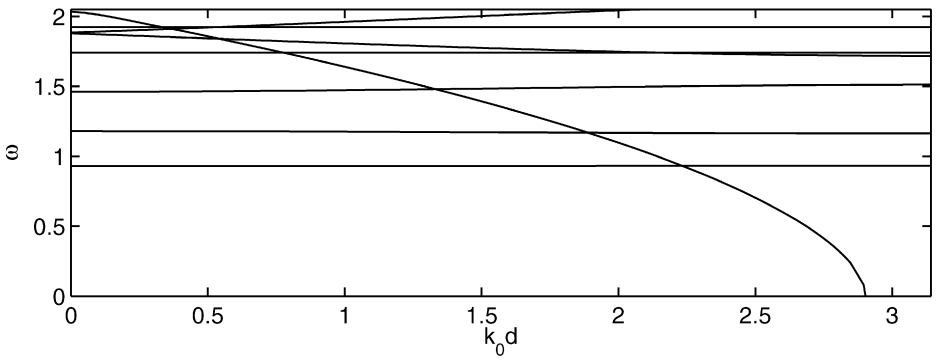

Fig. 6. Bloch spectrum for $\mu = 10$. We draw attention to the bending mode which begins at $k_0 d = 0$, $\omega \sim 2$ and has support on $0 \leqslant k_0 d \leqslant 2.9$. This mode attains a large gradient and thus permits rapid energy propagation.

group velocity throughout and are henceforth referred to as type II modes, examples of which are shown at $\mu = 1$, $\mu = 5$. Type I and II bending modes have a zero frequency, non-oscillatory solution at $k_0 = k_0^*$. Thirdly, certain values of μ yield modes with negative curvature which exist throughout the Brillouin zone, and such a mode is shown in the figure with $\mu = 0.5$, henceforth referred to as type III modes.

As $\mu \to \infty$, one obtains lowest mode solutions (that mode obtaining minimum frequencies) which intersect higher modes. As μ becomes larger, more modes are bounded below the bending mode at $k_0 d = 0$, permitting large group velocities even at high frequencies. In the limit $\mu = \infty$, equivalent to the clamped case, the bending mode disappears as it represents the zero-solution. We note also that these modes offer group velocities far above any other mode for large μ (e.g. $\mu = 5$), and hence permit rapid transmission of energy. We give an example of the bending mode for $\mu = 10$ in Fig. 6. The mode is not supported on the whole Brillouin zone, and obtainable at $0 \leqslant \omega \leqslant 2$. As a result of the vast frequency range occupied, the mode must obtain large group velocities (which are negative) throughout the Brillouin zone. This feature is especially apparent when contrasted against the almost dispersion-less modes supported by the structure, also shown in the figure at $\omega = 0.929, 1.179, 1.462$.

It is clear that as μ increases from 0, transition between types is possible, as $\mu = 0.2$ and $\mu = 2.5$ are of the same type, but $0.2 < \mu = 1 < 2.5$, of different type, exists at an intermediate value. We now turn our attention to identifying how this transition occurs as μ increases.

Fig. 7(a) shows the region of the first Brillouin zone on which the bending mode is supported as μ varies, and is shaded in the figure. Away from a number of critical μ the response is linear. The bending mode changes between the types described as μ increases. We note that type III modes are supported only on narrow regions, shaded darkly in the figure. At values $\mu = 0.481, 1.04, 1.53, 2.09, 2.58$, a transition occurs as bending modes to the left of these values disappear (the spectrum occupied by those modes shrinks to zero), and a new bending mode appears. This is marked by a discontinuity in the $k_0 d$ support and of the maximal ω over the mode at these values. Further, the switch at these values is between modes of positive and negative group velocities, thus if one were able to tune the guide through effective conditions, one could perturb about these values and so induce a rapid shift in the direction of energy

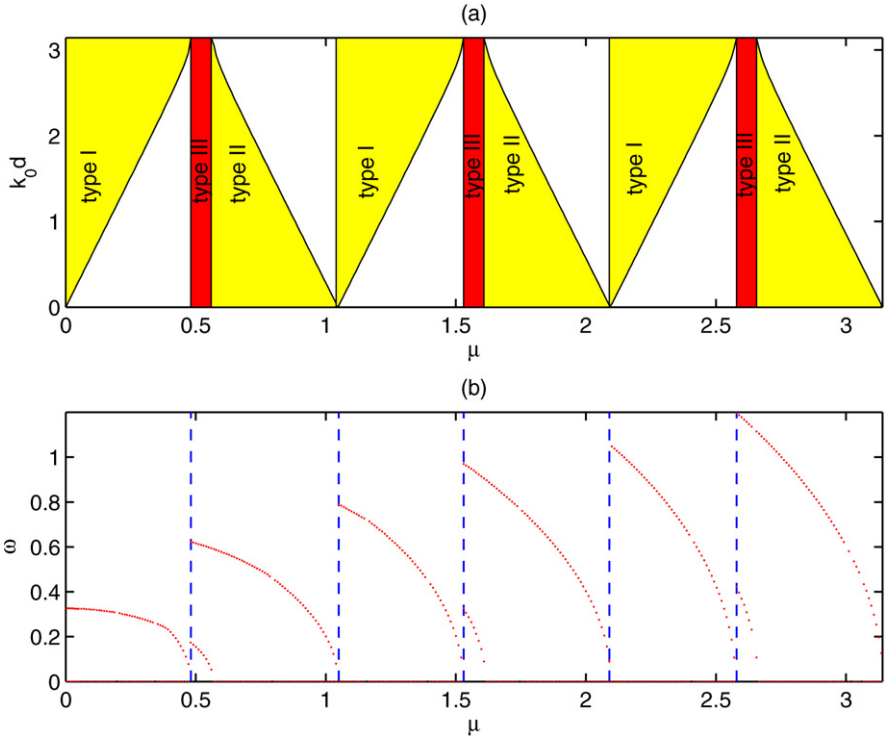

Fig. 7. Panel (a) shows the variation of the Bloch support of the bending mode as μ varies, and mode types are shown. Types I and II (existing only on some subset of the Brillouin zone) are shaded in light color, and type III modes are shaded darkly. Panel (b) shows the range of ω values occupied by the bending mode. Type I and II modes achieve $\omega = 0$ (non-propagating modes), and type III modes have positive lower bound, as shown.

propagation, and so yield potential applications in switching technology. Continuity as $\mu \to 0$ is observed, where, at the origin, the mode exists on all of $0 < k_0 d < \pi$. Fig. 7(b) shows the response of the maximal and minimal values of ω for the bending mode. It is worth noting that in straight walled guides, the width of the stopbands is determined by the dispersion relations at the edge of the Brillouin zone, [21]; these results also confirm our observations of modes having a uniformly signed group velocity throughout the Brillouin zone. Modes of types I and II are characterized by $\omega = 0$ minimal value of ω, shown in the figure. The critical impedance parameters, at which a new bending mode is formed, are shown as dashed vertical lines in the figure.

Fig. 8 shows the mode shape of the lowest mode for $\mu = 1$, in panels 8(a) and 8(c), and for $\mu = 0.2$ in panels 8(b) and 8(d). In the first of these cases, we examine the mode shape at $k_0 d = 0.286$ corresponding to the zero-frequency stationary solution of the bending mode, circled in Fig. 4. The second case is a mode whose support is on $1.21 < k_0 d < \pi$, as seen in Fig. 5, at $\omega = 0.305$ – at the edge of the Brillouin zone, and we see that despite differences in Bloch and impedance parameters, the response is similar between these cases. It is also noted that panel 8(b) shows the displacement response is linear in material 1. Careful examination of the lowest mode at various values of μ and $k_0 d$ shows that the shape across the guide is largely insensitive to changes in impedance, μ, and Bloch parameter k_0, and the examples presented here are typical of the bending mode. We also note the absence of symmetry across the guide, shown in panels (c) and (d), whereas symmetry/anti-symmetry is found in the clamped and traction-free cases.

4. Conclusions

We have investigated the Bloch spectrum of a straight, parallel walled acoustic guide subject to impedance boundary conditions on top and bottom. The focus has been on the special case in which $\mu_+ = -\mu_-$, and we have found that anomalous dispersion effects of the bending mode are possible, including negative curvature and existence only on some subset of the first Brillouin zone. Such effects can also be generated for $|\mu_+| \neq |\mu_-|$, provided they are of opposite signs, though unless $|\mu_+| = |\mu_-|$, the correspondence with the clamped case, given in Section 3, no longer

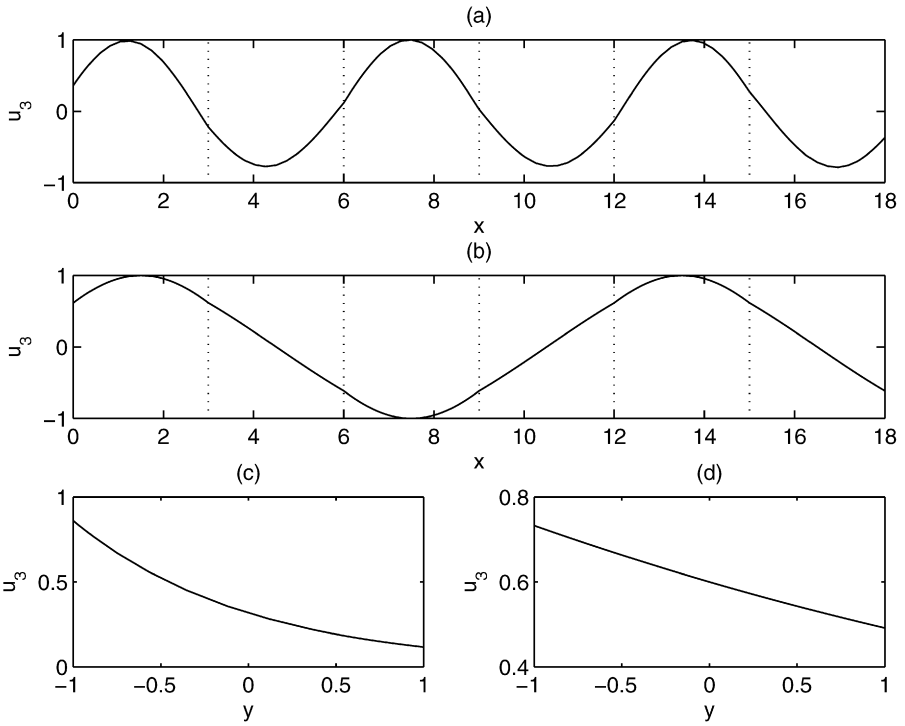

Fig. 8. Mode shapes along the guide are shown in (a), (b), and shapes across the guide are shown in (c), (d), for $\mu = 1$, $k_0 d = 0.286$ in panels (a), (c) and for $\mu = 0.2$, $k_0 d = \pi$ in (b), (d).

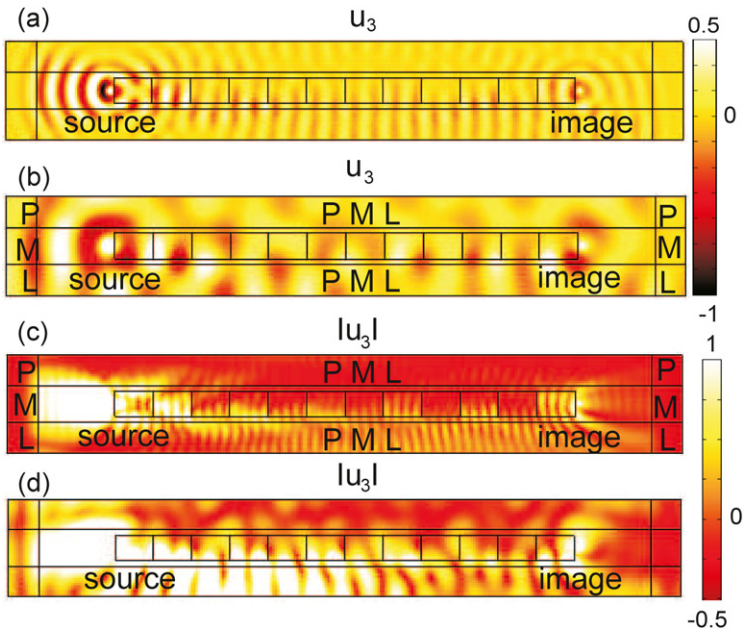

Fig. 9. Lensing effect for an acoustic line source of frequency $\omega = 4$ (panels a, c) and $\omega = 1.5$ (panels b, d) located on the left edge of a waveguide consisting of 6 cells of equal thickness $h = 2$ and length $d_1 + d_2 = 2d_1 = 6$ with impedance parameter $\mu = \pm 10$ on the guide walls, as in Fig. 6. Upper panel (a, b): 2D plot of the longitudinal displacement u_3; Lower panel (c, d): 2D plot of the absolute value $|u_3|$ of the longitudinal displacement; The high magnitude of the displacement on the bottom wall is notable.

holds as the symmetry is broken. We have described how these effects vary with boundary conditions on the guide walls, and focused on the response of the bending mode to these changes. Comparisons with the clamped case were drawn, and an explanation as to why negative bending mode group velocities are possible was given. There are potential applications in many areas, including a new generation of delay lines or high resolution medical imaging systems such as endoscopes for non-destructive imaging. Fig. 9 shows some preliminary results on a lensing effect using either the low frequency bending mode of Fig. 6 (panels b, d), or a higher-frequency mode (panels a, c), when $\mu = \pm 10$ on the top and bottom guide walls respectively. We believe that the effective impedance conditions assumed on the guide walls can be obtained through homogenization of corrugated waveguides. If one is interested in applications in electronic engineering, a design of electrical circuits such as in Fig. 1 will enable one to obtain dispersion curves as discussed in this paper in order to enable a better control of the signal wavespeed (through high or low group velocity). It is also interesting to note that the unusual behavior of the dispersion curve of the first bending mode which disappears or appears unexpectedly on finite segments strictly within the Brillouin zone clearly contradicts the widely accepted statement that width of gaps are controlled by the edges of the Brillouin zone, see [20,21].

References

[1] V.G. Veselago, The electrodynamics of substances with simultaneously negative value of ϵ and μ, Sov. Phys. Uspekhi 10 (1968) 509–514.
[2] J.B. Pendry, Negative refraction makes a perfect lens, Phys. Rev. Lett. 86 (2000) 3966.
[3] D. Maystre, S. Enoch, Perfect lenses made with left-handed materials: Alice's mirror? J. Opt. Soc. Am. A 21 (2004) 122–131.
[4] S.A. Ramakrishna, Physics of negative refraction, Rep. Prog. Phys. 68 (2005) 449.
[5] S.D.M. Adams, R.V. Craster, S. Guenneau, Bloch waves in multi-layered acoustic waveguides, Proc. R. Soc. London A 464 (2008) 2669–2692.
[6] A. Figotin, I. Vitebskiy, Slow light in photonic crystals, Waves Random Complex Media 16 (2006) 293–392.
[7] J.T. Mok, C.M. de Sterke, I.C.M. Littler, B.J. Eggleton, Dispersionless slow light using gap solitons, Nat. Phys. 2 (2006) 775–780.
[8] R.V. Craster, S. Guenneau, S.D.M. Adams, Mechanism for slow waves near cutoff frequencies in periodic waveguides, Phys. Rev. B 79 (2009) 045129.
[9] M. Saillard, D. Maystre, Scattering from metallic and dielectric rough surfaces, J. Opt. Soc. Am. A 7 (1990) 982–990.
[10] C. Caloz, T. Itoh, Electromagnetic Metamaterials: Transmission Line Theory and Microwave Applications, John Wiley and Sons, 2006.
[11] L. Brillouin, Wave Propagation in Periodic Structures, McGraw–Hill, 1946.
[12] J.R. Pierce, Traveling-Wave Tubes, D. Van Nostrand, 1950.
[13] J.B. Pendry, L. Martin-Moreno, F.J. Garcia-Vidal, Mimicking surface plasmons with structured surfaces, Science 305 (2004) 847–848.
[14] J.B. Pendry, A.J. Holden, D.J. Roberts, W.J. Stewart, IEEE Trans. Micr. Theory Techniques 47 (1999) 2075.
[15] W.B. Fraser, Orthogonality relation for the Rayleigh–Lamb modes of vibration of a plate, J. Acoust. Soc. Am. 59 (1976) 215–216.
[16] A.B. Movchan, N.V. Movchan, C.G. Poulton, Asymptotic Models of Fields in Dilute and Densely Packed Composites, ICP Press, London, 2002.
[17] R.L. Kronig, W.G. Penney, Quantum mechanics of electrons in crystal lattices, Proc. R. Soc. London 130 (1931) 499–531.
[18] A.B. Movchan, S. Guenneau, Split-ring resonators and localized modes, Phys. Rev. B 70 (2004) 125116.
[19] F. Zolla, G. Bouchitte, S. Guenneau, Pure currents in foliated waveguides, Q. J. Mech. Appl. Math. 61 (6) (2008) 453–474.
[20] J.L. Zhang, H.T. Jiang, S. Enoch, G. Tayeb, B. Gralak, M. Lequime, Two-dimensional complete band gaps in one-dimensional metal-dielectric periodic structures, Appl. Phys. Lett. 92 (2008) 053104.
[21] J.M. Harrison, P. Kuchment, A. Sobolev, B. Winn, On occurrence of spectral edges for periodic operators inside the Brillouin zone, J. Phys. A – Math. 40 (2007) 7597–7618.